Article

Journal of the Brazilian Chemical Society

https://dx.doi.org/10.21577/0103-5053.20240151

J. Braz. Chem. Soc. **2024**, *35*, 12, e-20240151, 1-14

Validation of Electrical Impedance Technique in Real-Time Using the xCELLigence as an Interference-Free Method for Assessing Cytotoxicity of Silver and Hydroxyapatite Nanoparticles

*Ekeveliny A. Veschi,[a] Wanderson de Souza,[a,b] Myrella K. G. Nobre,[a,b] Fernanda Sias,[a,b] Bárbara Gomes,[a,c] Beatriz L. Roquett,[a,c] Nathalia Müller,[a] Leonardo Boldrini,[a,c] Celso Sant'anna[a,b,c] and Jose Mauro Granjeiro[a,b,c]**

[a]*Laboratório de Biologia de Células Eucariontes, Diretoria de Metrologia Científica e Tecnológica, Instituto Nacional de Metrologia, Qualidade e Tecnologia, 25250-020 Duque de Caxias-RJ, Brazil*

[b]*Programa de Pós-Graduação em Biotecnologia, Instituto Nacional de Metrologia, Qualidade e Tecnologia, 25250-020 Duque de Caxias-RJ, Brazil*

[c]*Programa de Pós-Graduação em Biomedicina Translacional, Universidade do Grande Rio, 25071-202 Duque de Caxias-RJ, Brazil*

This study demonstrated the utility of real-time electrical impedance, utilizing the xCELLigence system to assess the cytotoxic effects of silver nanoparticles (AgNPs) and hydroxyapatite nanoparticles (HANPs) on A549 cells. Method validation confirmed the accuracy and reliability of cell index (CI) measurements. The NPs were thoroughly characterized to confirm their elemental composition, size, and morphology through energy dispersive spectroscopy, transmission electron microscopy, and dynamic light scattering. Cytotoxicity assays revealed a concentration-dependent response. Exposure to AgNPs resulted in a significant change in CI, with a pronounced increase followed by a sharp decrease in the first few hours after treatment at the highest concentration of 50 μg mL^{-1}. This pattern suggested an initial cell response to AgNPs exposure, possibly indicating mechanisms such as apoptosis or necrosis, followed by a decrease in cell adhesion. Conversely, HANPs demonstrated a tendency to restore CI at higher concentrations (1-100 μg mL^{-1}) before 48 h, suggesting a potential recovery in cell proliferation capacity. This underscores the diverse cell responses to NPs, emphasizing the sensitivity of the method in detecting subtle cytotoxic effects. These findings highlight the efficacy of real-time electrical impedance in dynamic nanoparticle cytotoxicity assessments, surpassing traditional assays. Adapting to high-throughput screening enhances nanomaterial safety evaluations.

Keywords: validation, nanotoxicity, hydroxyapatite nanoparticles, silver nanoparticles, electrical impedance, xCELLigence

Introduction

The testing of the cytotoxicity of nanoparticles (NPs) accurately and efficiently is challenging due to their complexity. These structures, measuring approximately 1-100 nm, are widely used because of their diverse properties, which benefit product development.[1-5] Before nanotechnology products are approved for use in humans, their cytotoxicity must be assessed. However, conventional methods often face limitations owing to interference from reagents, techniques, and NPs themselves, affecting the precision and objectivity of the results.[1,6] The interaction between NPs and chemical markers can lead to inconsistent results, as NPs may disrupt metabolic pathways or interfere with markers in cell culture or test media. The composition and properties of NPs can influence their interaction with chemical markers, potentially leading to contradictory results.[7] Chemical markers designed for specific cell parameters may experience interference from NPs, disrupting metabolic pathways.[8] Mello *et al.*[9] revealed that silver nanoparticles (AgNPs) with different sizes and coatings can interfere with spectroscopy-based assays, including 3-(4,5-dimethylthiazol-2-yl)-

*e-mail: jmgranjeiro@inmetro.gov.br
Editor handled this article: Ítalo O. Mazali (Guest)

2,5-diphenyltetrazoliumbromide (MTT), neutral red (NR), Hoechst, and resazurin, to varying extents. This suggests that their cytotoxicity may be either underestimated or overestimated. Additionally, the presence of NPs in culture or test medium can interfere with markers, yielding unreliable results.[10,11]

Given these challenges, there is an urgent need for new technologies that offer interference-free methods for a more reliable and comprehensive analysis of NPs cytotoxicity.[12-14] Real-time electrical impedance, as performed by the xCELLigence system, provides an alternative for assessing cell proliferation, a key cytotoxicity parameter, by monitoring cell proliferation in real-time without markers, thereby minimizing conventional method interference.[10,11,15] This technology represents a significant technological advance and supports nanotoxicology research by providing a deeper understanding of the dynamic interactions between cells and nanostructures.[16-19]

AgNPs and hydroxyapatite nanoparticles (HANPs) are two types of NPs with significant applications in the nanostructured products industry, from medical devices to water filters and dental materials.[9,20-23] Despite their benefits, concerns about their cytotoxicity persist, highlighting the importance of determining their safety range.[24-29] The lack of standardization and method validation in NPs cytotoxicity studies further complicates the definition of safe concentrations. Notably, both AgNPs and HANPs are present in inhalable products, raising concerns about lung cell homeostasis.[30-34] Thus, we selected AgNPs and HANPs as representative NPs because of their extensive usage across various industries and unique properties. It is crucial to assess cytotoxicity to ensure the safety of individuals exposed to these materials, including consumers and workers.

Therefore, this study proposes that the electrical impedance method validation using a real-time cell analyzer is a reliable and efficient method for evaluating the biological effects of NPs, eliminating the interference issues associated with conventional techniques.[30,35-38] By investigating the applicability of the xCELLigence system to AgNPs and HANPs in lung carcinoma cells (A549 cells), this study aims to contribute to the development of more robust and adaptable cell analytical methods for nanotoxicology, marking a significant advancement in the field.

Experimental

Cell culture

Here, we used the human lung carcinoma cell line A549 (ATCC CCL-185™), supplied by the Cell Bank of Rio de Janeiro (BCRJ, Rio de Janeiro, Brazil), packed in frozen ampoules and kept in liquid nitrogen. After thawing, cells were grown in high-glucose Dulbecco's modified Eagle's medium (DMEM) (Gibco Life Technologies, New York, USA) supplemented with 10% fetal bovine serum (FBS) (Gibco Life Technologies, New York, USA) at 37 °C in a humidified environment (CellXpert® C170i, Eppendorf, Hamburg, Germany) with 5% CO_2. Cell quantification was performed using a Neubauer chamber. Sterility was ensured by tests for bacteria, fungi, and mycoplasmas. For bacteria and fungi, the cell culture supernatant was placed in thioglycolate (TIO) (Acumedia, Baltimore, USA) and tryptic soy broth (TSB) (Acumedia, Baltimore, USA) and incubated aerobically for 14 days at 22.5 ± 2.5 °C and 32.5 ± 2.5 °C, respectively. Mycoplasma contamination in the cell supernatants was investigated by bioluminescence using the MycoAlert™ PLUS Mycoplasma Detection Kit (MycoAlert®, Lonza, Verviers, Belgium).

Experimental design and delimitation of dilution fractions (DF) for method validation

To validate the real-time cell analysis methodology using the xCELLigence equipment (RTCA SP Instrument, Roche, Mannheim, Germany), we used the experimental model presented in ABNT NBR ISO 20391-2.[39] Although this standard aims to analyze cell counting methods in suspension, we applied these experimental suggestions for validation. Considering the characteristics of A549 cells, we decided to use five dilution fractions, represented by DF = 0.15; 0.22; 0.28; 0.37; 0.44, resulting in suspensions containing 9.9×10^3, 1.5×10^4, 1.9×10^4, 2.5×10^4 and 3.0×10^4 cells mL^{-1}. Three representative replicates were produced from a single stock suspension containing 0.67×10^6 cells mL^{-1} for each dilution fraction. Each representative sample was analyzed in quadruplicate.

Improving pipetting accuracy and precision of cells

An independent study was conducted before planning the experimental validation (pre-evaluation) to verify pipetting accuracy. Using a calibrated analytical balance (AUW 220D, Shimadzu, Tokyo, Japan), we weighed the volumes of A549 cells and culture medium corresponding to each dilution fraction proposed in the experimental plan (0.15, 0.22, 0.28, 0.37, and 0.44) in triplicate. Reverse pipetting was performed using the same Eppendorf pipette and tip. The following formulas were used to calculate the pre-evaluated dilution fraction:

$$df_{(\text{pre-evaluated})} = \frac{\text{m1}}{\text{m1} + \text{m2}} \quad (1)$$

where m1 is the mass of the sample to be diluted (cell suspension), m2 is the mass of the pipetted diluent (DMEM containing 10% FBS), and

$$df_{(\text{pre-evaluated})} = \beta_{\text{pipetting}} \times df_i + \in_{ij} \quad (2)$$

where $\beta_{\text{pipetting}}$ is a constant verified by the slope of the curve for the targeted dilution fraction (df_i), and $\in_{ij}$ represents the deviation of $df_{(\text{pre-evaluated})}$ from the proportional trend.

Real-time impedance monitoring using xCELLigence for method validation

The equipment was designed to monitor the cell behavior in real-time and record its influence on the electrical impedance. The software was installed on a computer connected to the equipment that automatically generated and processed four sets of data to monitor cell physiological parameters continuously. Following the manufacturer's recommendations, we initially checked the system using a resistor board to ensure proper functioning (RTCA MP Instrument Operator Manual, Roche, Mannheim, Germany). Once confirmed, we calibrated the system by introducing an experimental E-plate 96 PET (ACEA Biosciences, San Diego, USA) containing only 50 µL of the DMEM 10% FBS. Subsequently, 100 µL of each cell suspension was added according to the dilutions fractions, DF = 0.15; 0.22; 0.28; 0.37; 0.44. To minimize operator bias and selection, we coded the dilution fractions. The instrument was programmed to monitor the cells for 96 h and record the electrical impedance values every hour to obtain the cell growth pattern.

The process of evaluating performance parameters for validating a method

The method was evaluated based on two performance parameters: tendency and precision.[40] For this purpose, the cell index (CI) values were measured after 2 h of cell plating, and those obtained after 24 h of analysis were used. Data were automatically generated and processed using the software installed on a computer connected to the equipment. Statistical analyses were conducted using GraphPad Prism 9,[41] Excel,[42] and the Comet Score software: Counting Method Evaluation Tool,[43] developed by the National Institute of Standards and Technology (NIST).

Synthesis and physicochemical characterization of AgNPs and HANPs

AgNPs and HANPs were used in this study. The AgNPs (Carboprata®, São Paulo, Brazil) was synthesized by electrolysis using a silver metal rod, water, and CO_2. The HANPs used in this study was a certified reference material (CRM 7966.0001) produced and provided by the Inorganic Analysis Laboratory (Labin) of the Chemical Metrology Division of INMETRO (Duque de Caxias, Brazil).[44] The reaction between calcium nitrate tetrahydrate and diammonium hydrogen phosphate synthesized them. The calcium-phosphorus (Ca/P) molar ratio of this material corresponded to the theoretical molar ratio of 1.67, which is the stoichiometric composition of HANPs with the chemical formula $Ca_{10}(PO_4)_6(OH)_2$.

Following the synthesis of AgNPs and HANPs, physicochemical characterization of the NPs was conducted through the following experiments.

Energy dispersive spectroscopy (EDS)

The elemental identification of AgNPs and HANPs was conducted post-synthesis using EDS coupled to an FEI Magellan 400 scanning electron microscope at 10 kV (FEI Company, Oregon, USA). First, 2 mL of the NPs solution was centrifuged at 25,200 × g for 20 min. The resulting pellet was dried in an oven at 60 °C for 60 min and then placed on the carbon band of the matrix.

Transmission electron microscopy (TEM)

The morphology and agglomeration of AgNPs and HANPs were evaluated post-synthesis using TEM. First, 5 µL of the NPs solution (AgNPs and HANPs) were analyzed at a concentration of 0.5 mg mL^{-1} diluted in ultrapure water, and the culture medium (DMEM high glucose) was deposited on 250 mesh copper grids coated with Formvar and dried at room temperature. Subsequently, images were captured using TEM (Tecnai G2 Spirit FEI Company, Oregon, USA) at 120 kV.

Dynamic light scattering (DLS)

The particle size distribution (nm) and surface charge (zeta potential analysis (ζ (mV)) of AgNPs and HANPs were investigated using DLS with a ZetaSizer Nano ZS (Malvern Instruments GmbH, Worcestershire, United Kingdom). AgNPs and HANPs were analyzed at a 0.5 mg mL^{-1} concentration, diluted in ultrapure water and culture medium (DMEM high glucose). DLS measurements were conducted at 25 °C using disposable optical polystyrene cuvettes (10 mm in size). DLS measurements were performed in triplicate for each condition tested, and the instrument software automatically determined the number

and duration of the partial measurements for each run. Prior to each measurement, the suspension was homogenized by pipetting several times to ensure uniformity.

Real-time monitoring of cell proliferation by impedance after method validation

To evaluate the cytotoxicity of AgNPs and HANPs, approximately 1.5 × 10^4 A549 cells were seeded into each well. After 24 h, the cells were treated with different concentrations of AgNPs (0.05, 0.1, 0.5, 1.0, 5.0, 10, 30, and 50 μg mL^{-1}) and HANPs (0.01, 0.05, 0.1, 0.5, 1.0, 10, 50, and 100 μg mL^{-1}) for 48 h, totaling 72 h for the experiment. The negative control consisted of cells cultured in a biological basal medium without NPs treatment. The positive control included cells cultured in biological basal medium without NPs treatment and treated with 1% Triton after 24 h of cultivation. The CI changes were analyzed using xCELLigence software (RTCA SP Instrument, Roche, Mannheim, Germany).

Statistical analysis

Data are expressed as means ± 95% confidence intervals. The normality of the distribution of the samples was assessed using the Shapiro-Wilk test, and the statistical significance of the data was determined using one-way analysis of variance (ANOVA) (Dunnett's test was used to compare various treatments with a control group) and an unpaired *t*-test. Statistical significance was defined as a *p*-value of < 0.05. Each experiment was conducted in triplicate and repeated thrice independently.

Results

Validation of real-time impedance monitoring method using xCELLigence

Initially, we aimed to ascertain whether pipetting inaccuracies resulting from incorrect estimates of pipetted suspension volumes could affect the reliability of DF. A separate pre-evaluation study was conducted before experimental planning, adhering to specific acceptance standards to achieve this. Thus, the pre-evaluation of dilution integrity aimed to replicate the planned experimental procedure faithfully. Utilizing the recorded mass of the cell suspension and the mass of the pipetted diluent, culture medium containing 10% FBS, we calculated the pre-evaluated dilution factor ($fd_{ij}^{pre\text{-}evaluated}$) for each sample (Figure 1a), assuming similar densities of the sample to be diluted and the dilution medium.

During the validation experiment, electrical impedance

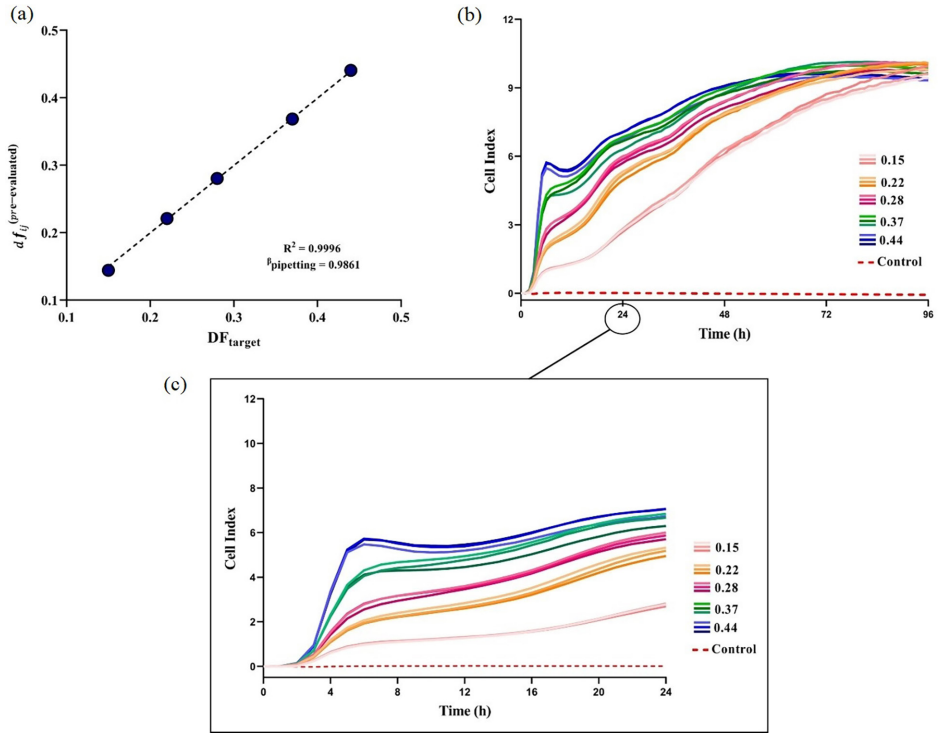

Figure 1. Variation in cell index (CI) at different concentrations in A549 cells. (a) Linear regression of pre-evaluated target dilution values as a function of target dilution fraction for pipetting integrity assessment; (b) Various cell dilution fractions were utilized and analyzed in xCELLigence: 0.15 (light pink), 0.22 (orange), 0.28 (dark pink), 0.37 (green), and 0.44 (blue) in 96-h data; (c) the same curve of (b), focusing on the first 24 h. The control corresponds to the measured values of the culture medium supplemented with 10% FBS without adding cells and is depicted in red. Representative data are from three independent experiments.

measurements were continuously recorded on the xCELLigence equipment for 96 h, resulting in the CI. However, for the analysis of performance parameters, only the CI values corresponding to the 2 and 24 h marks of the experiment were considered (see Figure 1b). Upon analyzing the experimental curves for each dilution fraction, we observed initial cell adhesion to the wells, which increased the recorded CI. Subsequently, we observed an exponential growth phase, known as the logarithmic growth phase, during which the cells multiplied rapidly until they reached a proliferation plateau. These phases directly correlated with the number of cells in each well (Figure 1b). Each dilution fraction displayed varying times and CI values for each phase.

Emphasizing the significance of analyzing CI values recorded within the first 2 and 24 h of the experiment is crucial for the intended use of this technique. This approach facilitates the evaluation of cell behavior during the initial adhesion and logarithmic phases, providing valuable insights into cell development over time. Such information is essential for assessing the quality and guiding decision-making in subsequent experiments conducted with the cells (Figure 1c).

As previously mentioned, the method validation process focused on two analysis periods: 2 and 24 h. To ensure reliable and accurate results, analytical method validation involves the evaluation of various performance parameters.[45] In this context, the trend was determined using the coefficient of determination (R^2) and proportionality index (PI) calculated from the COMET application shown in Table 1.

Table 1. Displays the coefficient of determination (R^2) and proportionality index (PI)

Parameter	time	
	2 h	24 h
R^2	0.99	0.98
PI	0.68	1.84

The method's precision was verified by calculating the coefficient of variation (CV), in the same application (Figure 2).

The acceptance criteria for each parameter are presented in Table 2.

Real-time impedance AgNPs cytotoxicity monitoring after method validation

An analysis was carried out using EDS in conjunction with SEM to determine the elemental composition of

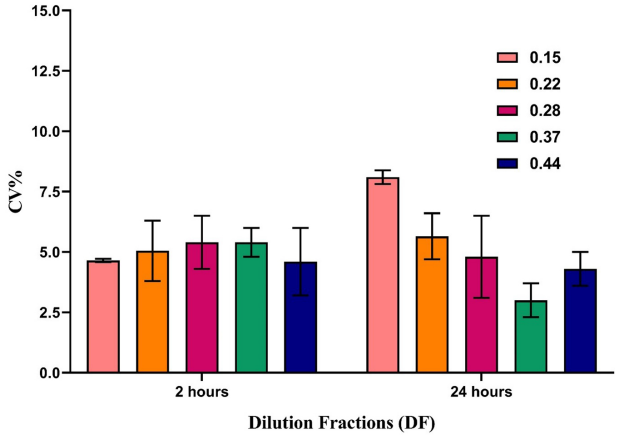

Figure 2. Performance parameters for method validation. The graph shows the coefficient of variation for 2 and 24 h. The results represent the mean ± 95% confidence intervals of three independent experiments performed in triplicates.

Table 2. Outlines the acceptance criteria for the validation parameters

Performance parameter	Analyzed parameter	Acceptance criteria
Trend	R^2	$R^2 \geq 0.98$
	PI	PI ≤ 2.0
Precision	CV	CV ≤ 20%

R^2: coefficient of determination; PI: proportionality index; CV: coefficient of variation.

AgNPs. The analyses were performed with the NPs pellet in the region of interest represented by a yellow asterisk and yielded a spectrum related to the intensity and energy (keV). In the spectrum of AgNPs samples (60 μg mL^{-1}), carbon (C), oxygen (O), fluorine (F), silicon (Si), aluminum (Al), and silver (Ag) are present (Figure 3a).

Moreover, transmission electron microscopy revealed the presence of AgNPs with a primary size of 45 nm and equiaxed and spheroidal morphologies (Figure 3b). However, owing to its high reactivity, there were a small number of AgNPs agglomerates after interaction with the culture medium (DMEM high glucose) (Figure 3c).

The average hydrodynamic size (expressed in nm) and zeta potential (expressed in ζ (mV)) of the AgNPs were determined by DLS, both when diluted in ultrapure water and culture medium (DMEM high glucose). The AgNPs diluted in ultrapure water at a 60 μg mL^{-1} concentration exhibited an average hydrodynamic size of 75.79 ± 0.33 nm, with a polydispersity index (PDI) of 0.49 ± 0.06 (Figure 3d). After this initial analysis, a measurement was performed in DMEM high glucose with 10% (v/v) FBS, which revealed a significant increase in both the average hydrodynamic size, which increased to 122.4 ± 2.94 nm, and the PDI, which reached 0.56 ± 0.02 (Figure 3d).

The zeta potential (ζ (mV)) reflects the extent of electrostatic attraction or repulsion between the NPs in the

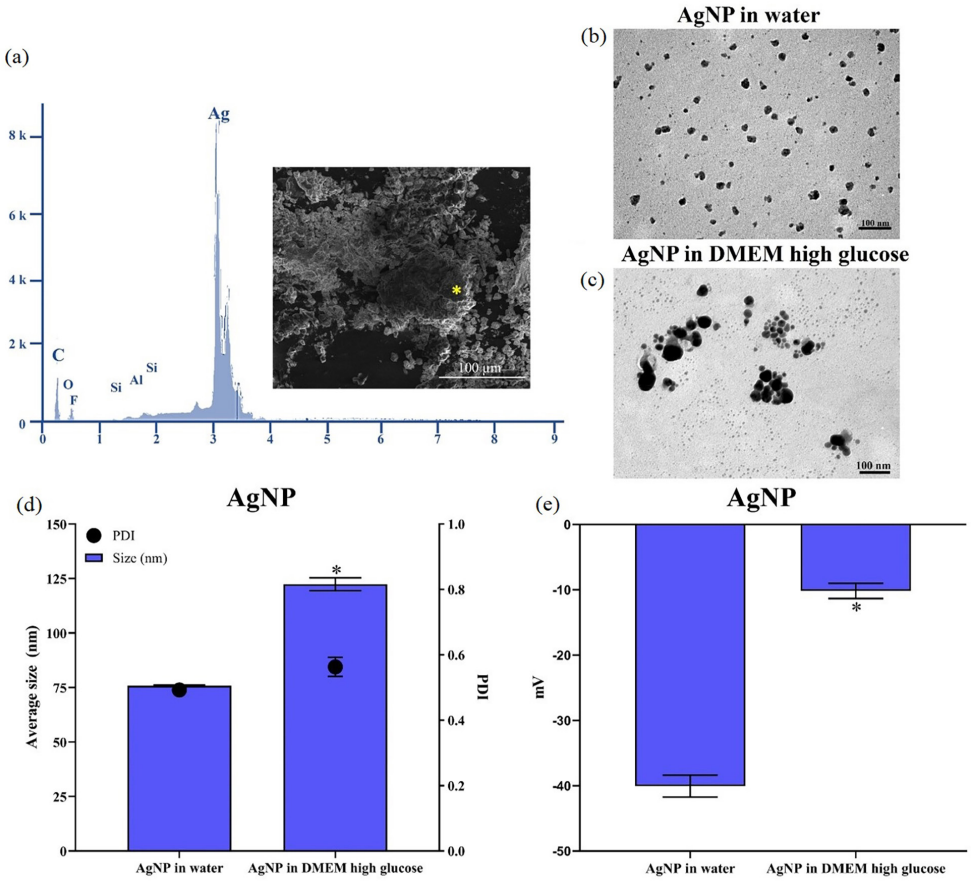

Figure 3. Physicochemical characterization of AgNPs. (a) The elemental composition of AgNPs was analyzed using EDS in conjunction with SEM. The agglomeration state and morphology were examined by transmission electron microscopy (TEM) in both (b) ultrapure water and (c) DMEM high glucose (biological media), scale bar 100 nm; (d) the average hydrodynamic size (nm) of AgNPs and the polydispersity index (PDI) were determined by DLS. PDI values close to zero were considered ideal; (e) the surface charge of AgNPs in 0.01 M PBS and DMEM high glucose was determined by DLS. The zeta potential of the solution is given by ζ (mV). The results represent the mean ± 95% confidence intervals of three independent experiments performed in triplicates. Statistical differences ($p < 0.05$; unpaired *t*-test) between the groups marked with * (AgNPs in water *versus* AgNPs in DMEM high glucose) were considered significant.

suspension. Thus, it can be shown whether NPs solutions exhibit charge stability, which often reduces the formation of agglomerates and aggregates. Therefore, AgNPs in ultrapure water showed a surface charge of –40.1 ± 1.6 mV (Figure 3e). After contact with DMEM high glucose, the AgNPs surface charge decreased significantly to –10.1 ± 1.1 mV.

Figure 4a illustrates the analysis of A549 cell proliferation based on CI values using electrical impedance on the xCELLigence device. A549 cells were treated with various concentrations of AgNPs (0.05, 0.1, 0.5, 1, 5, 10, 30, and 50 µg mL^{-1}) for 48 h. After treatment with AgNPs at the highest concentration (50 µg mL^{-1}), a decrease in CI was observed compared to the negative control (cells cultured with medium alone). Notably, an initial increase in CI was observed in A549 cells after treatment with 30 and 50 µg mL^{-1}, reaching a maximum CI after 5 h of treatment (CI ca. 17) at 50 µg mL^{-1}. However, a subsequent decline in CI values was observed. After 12 h of treatment, a concentration of 50 µg mL^{-1} significantly reduced CI compared to the negative control. In contrast, the effect of AgNPs at 30 µg mL^{-1} was partially reversed, reaching a CI equivalent to that of the negative control after 7 h of treatment. Other concentrations of AgNPs did not significantly affect CI over time compared to the control. Additionally, a decrease in CI was observed in the positive cell death control (cells treated with TritonTM X-100 0.1%), demonstrating the capability of the device to assess cell parameters.

Figure 4b compares the CI values between different concentrations of AgNPs and the negative control (cells cultured in medium alone) after 48 h of treatment. Treatment with 50 µg mL^{-1} AgNPs resulted in a 36% reduction in CI compared with the negative control.

Real-time impedance HANPs cytotoxicity monitoring after method validation

The elemental composition of HANPs was examined using EDS in conjunction with SEM. The analysis generated

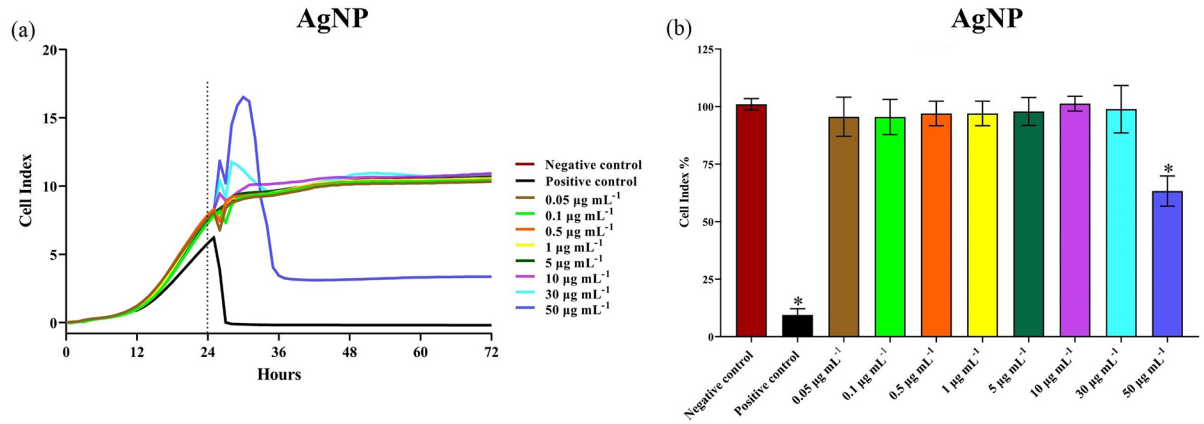

Figure 4. Proliferation of A459 cells after treatment with AgNPs. (a) The cell index (CI) of A549 cells was evaluated using real-time electrical impedance on an xCELLigence device after the interaction with AgNPs. Different concentrations of AgNPs (0.05, 0.1, 0.5, 1, 5, 10, 30, and 50 µg mL^{-1}) were applied for 48 h. The negative control represents cells cultured in DMEM high glucose without AgNPs treatment, whereas the positive control represents cells cultured in the same medium, but treated with 1% Triton after 24 h; (b) the bar graph shows the percentage of CI of A549 cells normalized to the negative control after treatment with AgNPs. The results represent the mean ± 95% confidence intervals of three independent experiments performed in triplicates. Statistical differences ($p < 0.05$; one-way ANOVA) between groups marked with * (50 µg mL^{-1} *versus* negative control) were considered significant.

a spectrum correlating intensity and energy (keV), revealing the presence of carbon (C), oxygen (O), calcium (Ca), and phosphorus (P) in the HANPs samples (Figure 5a).

Transmission electron micrographs in ultrapure water (Figure 5b) and the culture medium (Figure 5c) showed HANPs with a primary size of 200 nm and rod morphology. However, owing to their hydrophobic properties and high reactivity, HANPs tended to form clusters, as identified by DLS (Figure 5d).

The average hydrodynamic size and zeta potential of the HANPs were determined using DLS in ultrapure water and culture medium. HANPs diluted in ultrapure water at a concentration of 1 mg mL^{-1} exhibited an average hydrodynamic size of 1457.60 ± 337.10 nm, with a PDI of 0.50 ± 0.88 (Figure 5d). Subsequent measurements in DMEM high glucose with 10% (v/v) FBS showed a significant increase in both mean hydrodynamic size (1093.33 ± 31.78 nm) and PDI (0.50 ± 0.01).

Regarding zeta potential, HANPs in ultrapure water displayed a surface charge of –23.1 ± 0.4 mV, which decreased significantly to –10.2 ± 1.3 mV after exposure to DMEM high glucose.

Analysis of cell proliferation based on CI was also performed using HANPs. A549 cells were treated with HANPs for 48 h. After 24 h of plating, the cells were exposed to different concentrations of HANPs (0.01, 0.05, 0.1, 0.5, 1, 10, 50, and 100 µg mL^{-1}). Consequently, a decrease in the CI of A549 cells compared to that of the negative control (cells in culture medium) was observed at a concentration of 1 µg mL^{-1}, which was even more pronounced at 100 µg mL^{-1} (Figure 6a). These findings are summarized in Figure 6b (which refers to data only after 48 h of treatment), where it is evident that 100 µg mL^{-1} HANPs reduced CI by 39.8% compared to the negative control. It should be noted that at approximately 50 h for concentrations of 1, 10, and 50 µg mL^{-1} and 40 h for 100 µg mL^{-1}, the CI increased over time, suggesting a recovery in the cell proliferation capacity.

Discussion

Nanotoxicology is a key field of science that focuses on understanding the potentially harmful effects of NPs on human health. Several methods have been established to evaluate NPs cytotoxicity, among which electrical impedance has proven to be an effective tool for the accurate assessment of NPs impact on cellular behavior.[46,47] Traditional cytotoxicity assessments, such as MTT, MTS (3-(4,5-dimethylthiazol-2-yl)-5-(3-carboxymethoxyphenyl)-2-(4-sulfophenyl)-2*H*-tetrazolium), lactate dehydrogenase (LDH), neutral red, and apoptosis assays, can be influenced by interactions with NPs, sometimes leading to inaccurate results.[7,8,12]

Electrical impedance, measuring the electrical resistance and capacitance changes of cells when exposed to NPs, offers a non-invasive and real-time analysis, allowing for the continuous observation of cell behavior.[10,11,15,48] This method also measures the CI, an indicator closely associated with cell proliferation.[49-51] Its high sensitivity and specificity make electrical impedance particularly adept at detecting early cytotoxic changes in cells, potentially before such effects are visible through other methods.[52-55]

Hence, in this study, we aimed to validate and explore the utility of electrical impedance for assessing the cytotoxicity of the A549 cells exposed to AgNPs and HANPs.

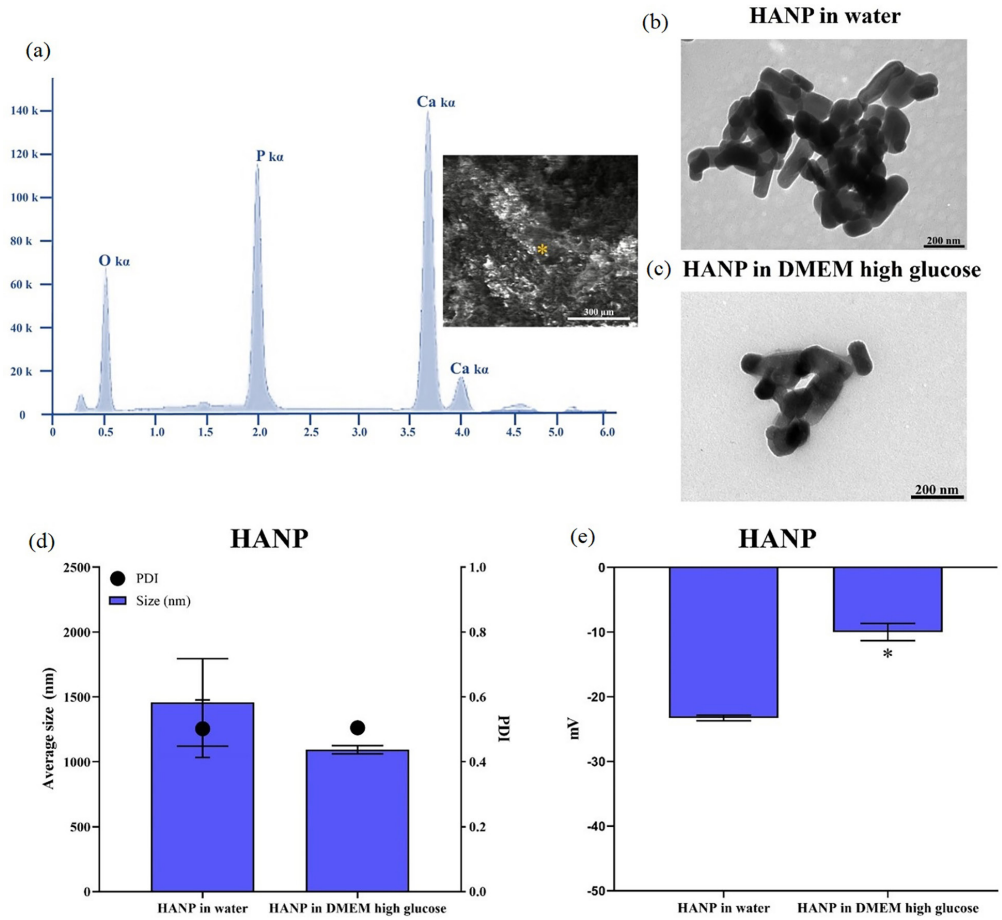

Figure 5. Physicochemical characterization of HANPs. (a) The elemental composition of HANPs was analyzed using EDS in conjunction with SEM; (b) TEM images of HANPs in ultrapure water; (c) TEM images of HANPs in high-glucose DMEM (biological medium). Scale bar: 200 nm; (d) the average hydrodynamic size (nm) of HANPs and the polydispersity index (PDI) were determined using DLS. PDI values close to zero were considered ideal; (e) the surface charge of HANPs in 0.01 M PBS and DMEM high glucose was determined by DLS; the zeta potential of the solution is given in ζ (mV). The results represent the mean ± 95% confidence intervals of three independent experiments performed in triplicate. Statistical differences ($p < 0.05$; unpaired *t*-test) between the groups marked with * (AgNPs in water *versus* AgNPs in DMEM high glucose) were considered significant.

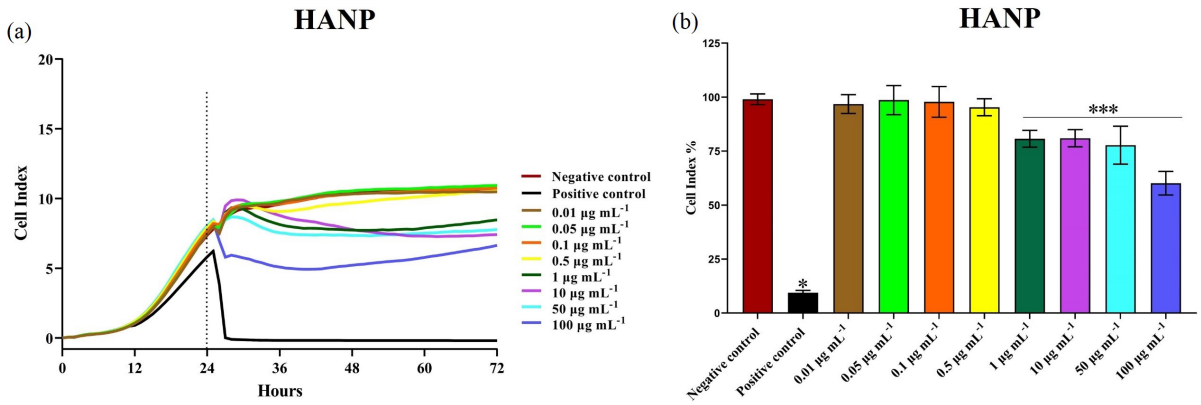

Figure 6. Proliferation of A459 cells after treatment with HANPs. (a) The cell index (CI) of A549 cells after interaction with HANPs was assessed using real-time electrical impedance on xCELLigence. Different concentrations (0.01, 0.05, 0.1, 0.5, 1, 10, 50, and 100 µg mL^{-1}) were used for 48 h. The negative control corresponded to cells cultured in a biological basal medium without HANPs treatment. The positive control corresponded to cells cultured in biological basal medium without HANPs and treated with 1% Triton after 24 h of cultivation; (b) the bar graph normalized to the control (negative control) shows the percentage of CI in A549 cells after treatment with HANPs. The results represent the mean ± 95% confidence intervals of three independent experiments performed in triplicates. Statistical differences ($p < 0.05$; one-way ANOVA) between the groups marked with * (1, 10, 50, and 100 µg mL^{-1} *versus* the negative control) were considered significant.

Method validation is essential before conducting cytotoxicity assays, ensuring reliability and suitability for intended purposes.[56] According to the International Vocabulary of Metrology (VIM)[57] and ABNT ISO/IEC 17025:2017,[58] validation confirms that specific requirements are met through examination and objective evidence. This process involves assessing various performance parameters to ensure the precision and reliability of results. Validating biological processes can be more complex than analytical methods, requiring evaluation of both analytical and biological parameters.[59,60]

To validate the xCELLigence equipment, we followed the recommendations of ABNT NBR ISO 20391-2 recommendations.[39] We assessed pipetting errors, which are crucial for maintaining DF integrity.[61] Results met ISO 20391-2 standards, showing R^2 and $\beta_{pipetting}$ values over 0.98, indicating excellent performance.[61] Exceptional data sets were observed at 2 and 24-h intervals, with PI values below 2.0, ensuring result reliability.[40] Maintaining accuracy in dilution fraction relationships is vital for interpreting biological processes accurately. CV values below 20% affirmed measurement uniformity, precision, and reliability.[40,62]

AgNPs and HANPs are extensively utilized in products and applications that may affect the respiratory system.[20,63,64] In this study, we evaluated the cytotoxicity of AgNPs, which is widely used across industries due to its unique properties.[65-67] Exposure to AgNPs primarily occurs through consumer products, such as medical devices and respiratory products,[9,20,21] during their manufacturing or after improper disposal.[68-72] Scientific evidence links AgNPs exposure to toxic effects on various body cells and DNA (deoxyribonucleic acid) interactions,[73-75] leading to oxidative stress, inflammation, and alterations in gene expression.[24,76] However, inconsistencies in outcomes persist. The adoption of reliable techniques, such as real-time electrical impedance, helps address uncertainties in AgNPs cytotoxicity assessment. On the other hand, HANPs is commonly found in dental materials and orthopedic implants, serving as a coating material for titanium implants, grafting material in tissue engineering, and remineralizing agent in preventive dentistry.[22,23]

Therefore, investigating the cytotoxicity of these NPs in lung cells is imperative for assessing their potential adverse effects under both environmental and working conditions. Secondly, lung cells play a crucial role in evaluating the toxicity of inhalable materials, as they are the primary cells exposed to inhaled airborne particles.[32,33] Due to their similar phenotype and response to lung stimuli, A549 cells are a suitable lineage for *in vitro* toxicity studies.[77,78]

Initially, AgNPs and HANPs were characterized using EDS-SEM, TEM, and DLS following the ISO 19337 standard.[79] The EDS-SEM analysis confirmed the elemental composition of AgNPs and HANPs. The carbon likely originated from the carbon tape used to fix the samples, whereas the other elements may have originated from the production process of AgNPs.

In this study, TEM and DLS tests were used to assess the effect of the culture medium (DMEM high glucose supplemented with FBS) on NPs size, agglomeration, and morphology. The presence of proteins and ions in the medium promoted the formation of a protein corona around the NPs. Studies[80] have shown that this nano-bio-interface significantly affects NPs size, uptake, internalization, and transport into cells.

DMEM high glucose supplemented with FBS increased the average hydrodynamic size of AgNPs to 122.4 nm compared to water (75.79 nm), concomitant with a decrease in zeta potential, suggesting the formation of a protein corona.[81-85] Consistently, our results revealed a reduction in the surface charge of both AgNPs (from –40.1 to –10.1 mV) and HANPs (from –23.1 to –10.2 mV) upon exposure to DMEM high glucose supplemented with FBS.

Conversely, protein corona formation appeared to stabilize HANPs, as evidenced by a decrease in hydrodynamic size compared to NPs diluted in water (decrease from 1457.60 to 1093.33 nm). Despite being hydrophobic in its pure form, HANPs may exhibit more hydrophilic properties in biological applications because of its altered crystalline structure and surface contamination.[86-88] The hydrophobic properties of HANPs can significantly affect its dispersion in biological culture media. Dispersing HANPs in a biological medium such as DMEM with high glucose supplemented with FBS may alter the average size and dispersion of the NPs.[89] The presence of proteins in the culture medium can significantly alter the surface properties of HANPs through adsorption, making them more hydrophilic and improving their dispersion in solution.[82,90-94] The protein corona can enhance the colloidal stability of particles and prevent their aggregation, resulting in a smaller average size.[95-98] However, it should be noted that the effects of dilution in the culture medium on the hydrophobicity and average size of HANPs can be influenced by factors such as protein concentration, pH, ionic strength, and temperature.[99-102] Therefore, further studies are required to fully understand how these factors interact with each other and influence the properties of HANPs.

DLS is effective for analyzing rounded NPs because of its assumption of a spherical size distribution and reliance on Brownian motion.[103,104] However, non-spherical shapes, such as rod-shaped NPs (e.g., HANPs), pose challenges

for DLS analysis because of their anisotropic Brownian motion.[104,105] This motion, dominated by movement along the long axis, can lead to the overestimation of particle size.[105,106] In contrast, TEM provides more precise information about particle morphology and size. TEM analysis revealed AgNPs with a primary size of 45 nm and HANPs of approximately 200 nm, showing clusters that facilitated the identification of larger sizes using DLS.

AgNPs reduced the CI in A549 cells at a concentration of 50 μg mL^{-1}, as previously reported.[10] The decrease in CI indicates a reduction or loss of cell adhesion to the E-plate bottom, likely associated with cell death mechanisms. AgNPs can induce cell death through various mechanisms, including the release of Ag ions, endoplasmic reticulum stress, and the induction of apoptosis, autophagy, and necrosis.[107] Additionally, CI increased in the first 7 h following AgNPs treatment, attributable to morphological changes and hormesis.[108,109] It has been proposed that AgNPs may cause changes in cell morphology, affecting the cell membrane and cytoskeleton, leading to an increase in cell area and a decrease in cell motility and adhesion.[110-112] The interaction of AgNPs with the cell may also activate cell signaling pathways related to cell proliferation, leading to hormetic responses.[113] However, it is crucial to note that the hormesis effect may be temporary, and cytotoxic effects may prevail.[114]

In contrast, HANPs reduced CI at 1 μg mL^{-1} compared with the negative control, but it was non-cytotoxic. Although high calcium concentrations have been shown to be cytotoxic,[115] HANPs is very stable at the neutral pH used in our study.[116] An important aspect is the ability of HANPs to absorb nutrients from the culture medium, impacting cell metabolism and altering the CI. HANPs has a highly crystalline structure that enables the adsorption or retention of ions and molecules (such as amino acids, minerals, vitamins, and carbohydrates) from the cell culture medium.[117] This process is initiated by the physicochemical properties of the NPs surface, including the surface charge and specific surface area. Consequently, HANPs can serve as an adsorption system, capturing nutrients from the culture medium and diminishing their availability to cells.[118] We hypothesize that HANPs internalization might have affected cellular homeostasis and proliferation. Prior studies[119] have shown that HANPs uniquely adsorbs proteins and induces adverse effects on cell viability. Further studies with longer exposure times and functional analysis are desirable to address this behavior better.

Furthermore, we noticed cell recovery within 72 h despite the initial decrease in CI. Adaptation responses may lead to gene expression and protein production changes in some cells.[120]

Highlighting the potential of the xCELLigence system for nanomaterial toxicity screening, it is essential to note the 2021 publication of ISO/TS 21633 by the ISO.[121] This technical specification outlines the protocols for measuring electrical impedance in different *in vitro* cell-based systems, including general guidelines for NPs testing. Although studies on AgNPs effects on the Caco-2 intestinal cell line have been discussed, no research on HANPs has been conducted. This emphasizes the importance of our study in evaluating the effects of both AgNPs and HANPs on a relevant airway cell line.

While current studies have yielded intriguing findings on A549 cell behavior after treatment with AgNPs and HANPs, it is vital to recognize that these results are specific to the tested conditions and *in vitro* setup. Despite this limitation, it is essential to emphasize that real-time impedance monitoring offers continuous cell observation during NPs treatment, unlike traditional methods, such as colorimetric assays. This method enables the dynamic analysis of cell proliferation effects over time, facilitating the detection of process alterations. Thus, we acquired comprehensive insights into the different aspects of cell behavior in response to NPs treatment.

Conclusions

This study demonstrated the efficacy of the real-time electrical impedance method for detailed analysis of cell responses to NPs exposure, specifically AgNPs and HANPs. Methodological validation ensures accurate and reliable CI measurements and establishes a foundation for consistent and reliable results. Characterization of AgNPs and HANPs confirmed their identities and enabled observation of their distinct effects on A549 cell behavior. Notably, AgNPs exposure led to a rapid CI change, whereas HANPs showed potential CI normalization at higher concentrations before 48 h. These findings highlight the value of the real-time electrical impedance method in cytotoxicity studies, offering an advanced tool for dynamic, real-time analysis of cell-NPs interactions. This method surpasses traditional cytotoxicity assays by providing immediate insight into cell dynamics and responses.

Future research should extend this methodology to a broader range of NPs to further explore cell-NPs interactions. Investigating the molecular mechanisms of these interactions will deepen our understanding of NPs-induced cellular changes. Additionally, adapting this method for high-throughput screening can significantly enhance nanomaterial safety assessments, thereby ensuring the development of safe and effective nanotechnology applications.

Acknowledgments

Jose Mauro Granjeiro thanks CNPq (400030/2018-7) and INCT-regenera (465656/2014-5, supported by CNPq and FAPERJ) and project number FAPERJ E-26/10.000981/2019, Rede Nano/Saúde. Wanderson de Souza, mainly thanks to FAPERJ - E-26/204.586/2021 and 204.587/2021 (268814).

The authors would like to thank the Materials Metrology Division at INMETRO, especially the Microscopy Laboratory Center led by Braulio Soares Archanjo, for their help with the EDS-SEM analysis. The authors thank Ivone Andrade for her valuable help in obtaining the TEM micrographs. We would like to thank startup Carboprata®, especially Jonny Francisco Ros and Lígia Ferreira Gomes, for the synthesis of AgNPs and the technical support.

Author Contributions

Ekeveliny A. Veschi, Wanderson de Souza, Myrella Kenupp G. Nobre, and Jose Mauro Granjeiro designed the study. Ekeveliny A. Veschi, Wanderson de Souza, Myrella Kenupp G. Nobre, Fernanda Sias, Barbara Gomes, Beatriz L. Roquett, and Nathália Müller performed experimental work and analyses. Ekeveliny A. Veschi, Wanderson de Souza, Myrella Kenupp G. Nobre, Fernanda Sias, Barbara Gomes, Beatriz L. Roquett, Nathália Müller, Leonardo Boldrini, Celso Sant'anna and Jose Mauro Granjeiro contributed to technical support and discussion. Ekeveliny A. Veschi, Wanderson de Souza, Myrella Kenupp G. Nobre, and Jose Mauro Granjeiro wrote/edited the manuscript. All the authors contributed to the correction and management of the data presented in this work.

References

1. Jiang, C.; Liu, S.; Zhang, T.; Liu, Q.; Chen, W.; *Environ. Sci. Technol.* **2022**, *56*, 7426. [Crossref]
2. Teulon, J.-M.; Godon, C.; Chantalat, L.; Moriscot, C.; Cambedouzou, J.; Odorico, M.; Ravaux, J.; Podor, R.; Gerdil, A.; Habert, A.; Herlin-Boime, N.; Chen, S. W.; Pellequer, J.; *Nanomaterials* **2019**, *9*, 18. [Crossref]
3. Singh, V.; Yadav, S. S.; Chauhan, V.; Shukla, S.; Vishnolia, K. K. In *Diagnostic Applications of Health Intelligence and Surveillance Systems*; Yadav, D.; Bansal, A.; Bhatia, M.; Hooda, M.; Morato, J., eds.; IGI Global: Hershey, PA, 2021, p. 221-236. [Crossref]
4. Afolalu, S. A.; Okwilagwe, O.; Abdulkareem, A.; Emetere, M. E.; Ongbali, S. O.; Yusuf, O. O.; *IOP Conf. Ser.: Earth Environ. Sci.* **2021**, *665*, 012049. [Crossref]
5. Khaturia, S.; Chahar, M.; Sachdeva, H.; Sangeeta; Mahto, C. B.; *J. Nanomed. Nanotechnol.* **2020**, *11*, 543. [Crossref]
6. Kumar, A.; Dixit, C. K. In *Advances in Nanomedicine for the Delivery of Therapeutic Nucleic Acids*, 1st ed.; Nimesh, S.; Chandra, R.; Gupta, N., eds.; Woodhead Publishing: Cambridge, UK, 2017, ch. 3. [Crossref]
7. Taka, A. L.; Tata, C. M.; Klink, M. J.; Mbianda, X. Y.; Mtunzi, F. M.; Naidoo, E. B.; *Molecules* **2021**, *26*, 6536. [Crossref]
8. Liu, L.; Hao, Y.; Deng, D.; Xia, N.; *Nanomaterials* **2019**, *9*, 316. [Crossref]
9. Mello, D. F.; Trevisan, R.; Rivera, N.; Geitner, N. K.; Di Giulio, R. T.; Wiesner, M. R.; Hsu-Kim, H.; Meyer, J. N.; *Chem.-Biol. Interact.* **2020**, *315*, 108868. [Crossref]
10. Bernardo, L.; Corallo, L.; Caterini, J.; Su, J.; Gisonni-Lex, L.; Gajewska, B. U.; *PLoS One* **2021**, *16*, 0248491. [Crossref]
11. Yan, G.; Du, Q.; Wei, X.; Miozzi, J.; Kang, C.; Wang, J.; Han, X.; Pan, J.; Xie, H.; Chen, J.; Zhang, W.; *Molecules* **2018**, *23*, 3280. [Crossref]
12. Chang, C.-C.; Chen, C.-P.; Wu, T.-H.; Yang, C.-H.; Lin, C.-W.; Chen, C.-Y.; *Nanomaterials* **2019**, *9*, 861. [Crossref]
13. Vladitsi, M.; Nikolaou, C.; Kalogiouri, N. P.; Samanidou, V. F.; *Methods Protoc.* **2022**, *5*, 61. [Crossref]
14. Sun, Z.; Yang, J.; Li, H.; Wang, C.; Fletcher, C.; Li, J.; Zhan, Y.; Du, L.; Wang, F.; Jiang, Y.; *Biomaterials* **2021**, *274*, 120873. [Crossref]
15. Aguedo, J.; Lorencova, L.; Barath, M.; Farkas, P.; Tkac, J.; *Chemosensors* **2020**, *8*, 127. [Crossref]
16. Shinde, R. B.; Veerapandian, M.; Kaushik, A.; Manickam, P.; *Front. Bioeng. Biotechnol.* **2020**, *8*, 325. [Crossref]
17. Kermanizadeh, A.; Brown, D. M.; Møller, P. R.; *Nanomaterials for Food Applications*, 1st ed.; Rubio, A. L.; Rovira, M. J. F.; Sanz, M. M.; Gómez-Mascaraque, L. G., eds.; Elsevier: London, UK, 2019, ch. 12. [Crossref]
18. Villanueva-Flores, F.; Castro-Lugo, A.; Ramírez, O. T.; Palomares, L. A.; *Nanotechnology* **2020**, *31*, 132002. [Crossref]
19. Jash, P.; Parashar, R. K.; Fontanesi, C.; Mondal, P. C.; *Adv. Funct. Mater.* **2021**, *32*, 2109956. [Crossref]
20. Khatoon, N.; Mazumder, J. A.; Sardar, M.; *J. Nanosci.: Curr. Res.* **2017**, *2*, 107. [Crossref]
21. Botha, T. L.; Elemike, E. E.; Horn, S.; Onwudiwe, D. C.; Giesy, J. P.; Wepener, V.; *Sci. Rep.* **2019**, *9*, 4169. [Crossref]
22. Pajor, K.; Pajchel, L.; Kolmas, J.; *Materials* **2019**, *12*, 2683. [Crossref]
23. Bordea, I. R.; Candrea, S.; Alexescu, G. T.; Bran, S.; Băciuț, M.; Băciuț, G.; Lucaciu, O.; Dinu, C. M.; Todea, D. A.; *Drug Metab. Rev.* **2020**, *52*, 319. [Crossref]
24. Mao, B.-H.; Chen, Z.-Y.; Wang, Y.-J.; Yan, S.-J.; *Sci. Rep.* **2018**, *8*, 2445. [Crossref]
25. Rezvani, E.; Rafferty, A.; McGuinness, C.; Kennedy, J.; *Acta Biomater.* **2019**, *94*, 145. [Crossref]
26. Pulit-Prociak, J.; Grabowska, A.; Chwastowski, J.; Majka, T. M.; Banach, M.; *Colloids Surf., B* **2019**, *183*, 110416. [Crossref]

27. Labouta, H. I.; Asgarian, N.; Rinker, K. D.; Cramb, D. T.; *ACS Nano* **2019**, *13*, 1583. [Crossref]
28. Tirumala, M. G.; Anchi, P.; Raja, S.; Rachamalla, M.; Godugu, C.; *Front. Pharmacol.* **2021**, *12*, 612659. [Crossref]
29. Noga, M.; Milan, J.; Frydrych, A.; Jurowski, K.; *Int. J. Mol. Sci.* **2023**, *24*, 5133. [Crossref]
30. Saifi, M. A.; Khan, W.; Godugu, C.; *Pharm. Nanotechnol.* **2018**, *6*, 3. [Crossref]
31. Lekamge, S.; Ball, A. S.; Shukla, R.; Nugegoda, D. In *Reviews of Environmental Contamination and Toxicology*, vol. 248; de Voogt, P., ed.; Springer Nature: Cham, 2020, p. 1-80. [Crossref]
32. Tsoutsoulopoulos, A.; Gohlsch, K.; Möhle, N.; Breit, A.; Hoffmann, S.; Krischenowski, O.; Mückter, H.; Gudermann, T.; Thiermann, H.; Aufderheide, M.; Steinritz, D.; *J. Vis. Exp.* **2020**, *156*, e60572. [Crossref]
33. Hiemstra, P. S.; Grootaers, G.; van der Does, A. M.; Krul, C. A. M.; Kooter, I. M.; *Toxicol. In Vitro* **2018**, *47*, 137. [Crossref]
34. Holmila, R. J.; Vance, S. A.; King, S. B.; Tsang, A. W.; Singh, R.; Furdui, C. M.; *Antioxidants* **2019**, *8*, 552. [Crossref]
35. Le, H. T. N.; Kim, J.; Park, J.; Cho, S.; *BioChip J.* **2019**, *13*, 295. [Crossref]
36. Gu, Q.; Cuevas, E.; Ali, S. F.; Paule, M. G.; Krauthamer, V.; Jones, Y.; Zhang, Y.; *Int. J. Toxicol.* **2019**, *38*, 385. [Crossref]
37. Koklu, A.; Giuliani, J.; Monton, C.; Beskok, A.; *Anal. Chem.* **2020**, *92*, 7762. [Crossref]
38. Clérigo, F.; Ferreira, S.; Ladeira, C.; Marques-Ramos, A.; Almeida-Silva, M.; Mendes, L. A.; *Toxics* **2022**, *10*, 402. [Crossref]
39. ABNT NBR ISO 20391-2: *Biotecnologia — Contagem de Células - Parte 2: Planejamento Experimental e Análise Estatística para Quantificar o Desempenho do Método de Contagem*, INMETRO: Duque de Caxias, 2023.
40. Sarkar, S.; Lund, S. P.; Vyzasatya, R.; Vanguri, P.; Elliott, J. T.; Plant, A. L.; Lin-Gibson, S.; *Cytotherapy* **2017**, *19*, 1509. [Crossref]
41. *GraphPad Prism 9*; GraphPad Software Inc., San Diego, USA, 2020.
42. *Microsoft Excel*, version 16.0; Microsoft Corporation, Washington, USA, 2016.
43. Newton, D.; Lund, S.; *COMET*: Counting Method Evaluation Tool, Beta version; TriTek, Sumerduck, USA, 2024.
44. Instituto Nacional de Metrologia, Qualidade e Tecnologia (INMETRO); *Material de Referência Certificado DIMCI 0850*; Divisão de Metrologia de Materiais (Dimat): Duque de Caxias, 2023. [Link] accessed in July 2024
45. Instituto Nacional de Metrologia, Qualidade e Tecnologia (INMETRO); *Orientação sobre Validação de Métodos Analíticos: Documento de Orientação*; Coordenação Geral de Acreditação (CGCRE): Duque de Caxias, 2020. [Link] accessed in July 2024
46. Oberdörster, G.; Stone, V.; Donaldson, K.; *Nanotoxicology* **2007**, *1*, 2. [Crossref]
47. Cimpan, M. R.; Mordal, T.; Schölermann, J.; Allouni, Z. E.; Pliquett, U.; Cimpan, E.; *J. Phys.: Conf. Ser.* **2013**, *429*, 012026. [Crossref]
48. McAuley, E.; Mohanraj, B.; Phamduy, T.; Plopper, G. E.; Corr, D. T.; Chrisey, D. B.; *Int. J. Biomed. Nanosci. Nanotechnol.* **2011**, *2*, 136. [Crossref]
49. Ozdemir, A.; Ark, M.; *Niche J.* **2014**, *2*, 15. [Link] accessed in July 2024
50. Kho, D.; MacDonald, C.; Johnson, R.; Unsworth, C.; O'Carroll, S.; Du Mez, E.; Angel, C. E.; Graham, E. S.; *Biosensors* **2015**, *5*, 199. [Crossref]
51. Limame, R.; Wouters, A.; Pauwels, B.; Fransen, E.; Peeters, M.; Lardon, F.; De Wever, O.; Pauwels, P.; *PLoS One* **2012**, *7*, e46536. [Crossref]
52. Ponti, J.; Ceriotti, L.; Munaro, B.; Farina, M.; Munari, A.; Whelan, M.; Colpo, P.; Sabbioni, E.; Rossi, F.; *Altern. Lab. Anim.* **2006**, *34*, 515. [Crossref]
53. Ceriotti, L.; Ponti, J.; Colpo, P.; Sabbioni, E.; Rossi, F.; *Biosens. Bioelectron.* **2007**, *22*, 3057. [Crossref]
54. Kandasamy, K.; Choi, C. S.; Kim, S.; *Nanotechnology* **2010**, *21*, 375501. [Crossref]
55. Peper, J. K.; Schuster, H.; Löffler, M. W.; Schmid-Horch, B.; Rammensee, H.-G.; Stevanović, S.; *J. Immunol. Methods* **2014**, *405*, 192. [Crossref]
56. International Conference on Harmonisation of Technical Requirements for Registration of Pharmaceuticals for Human Use (ICH); *Validation of Analytical Procedures Q2(R2)*; ICH: London, 2023.
57. ABNT ISO/IEC Guide 99: *Vocabulário Internacional de Metrologia (VIM): Conceitos Básicos e Gerais e Termos Associados*, INMETRO: Duque de Caxias, 2012.
58. ABNT NBR ISO/IEC Guide 17025: *Requisitos Gerais para a Competência dos Laboratórios de Ensaio e Calibração*, INMETRO: Duque de Caxias, 2017.
59. Food and Drug Administration (FDA); *Analytical Procedures and Methods Validation for Drugs and Biologics: Guidance for Industry*; U.S. Department of Health and Human Services, Food and Drug Administration, Center for Drug Evaluation and Research (CDER), Center for Biologics Evaluation and Research (CBER): Silver Spring, 2015. [Link] accessed in July 2024
60. European Medicines Agency (EMA); *Guideline on Process Validation for the Manufacture of Biotechnology-Derived Active Substances and Data to be Provided in the Regulatory Submission*; Committee for Medicinal Products for Human Use (CHMP): London, 2012. [Link] accessed in July 2024
61. ISO Standard 20391-2: *Experimental Design and Statistical Analysis to Quantify Counting Method Performance*; ISO: Geneva, 2019.

62. Reed, G. F.; Lynn, F.; Meade, B. D.; *Clin. Vaccine Immunol.* **2002**, *9*, 1235. [Crossref]
63. Gherasim, O.; Puiu, R. A.; Bîrcă, A. C.; Burduşel, A.-C.; Grumezescu, A. M.; *Nanomaterials* **2020**, *10*, 2318. [Crossref]
64. Pangli, H.; Vatanpour, S.; Hortamani, S.; Jalili, R.; Ghahary, A.; *J. Burn Care Res.* **2021**, *42*, 785. [Crossref]
65. Fahmy, H. M.; Mosleh, A. M.; Elghany, A. A.; Shams-Eldin, E.; Serea, E. S. A.; Ali, S. A.; Shalan, A. E.; *RSC Adv.* **2019**, *9*, 20118. [Crossref]
66. Salleh, A.; Naomi, R.; Utami, N. D.; Mohammad, A. W.; Mahmoudi, E.; Mustafa, N.; Fauzi, M. B.; *Nanomaterials* **2020**, *10*, 1566. [Crossref]
67. Kareem, M. A.; Bello, I. T.; Shittu, H. A.; Awodele, M. K.; Adedokun, O.; Sanusi, Y. K.; *IOP Conf. Ser.: Mater. Sci. Eng.* **2020**, *805*, 012020. [Crossref]
68. Ferdous, Z.; Nemmar, A.; *Int. J. Mol. Sci.* **2020**, *21*, 2375. [Crossref]
69. Adawi, H. I.; Newbold, M. A.; Reed, J. M.; Vance, M. E.; Feitshans, I. L.; Bickford, L. R.; Lewinski, N. A.; *NanoImpact* **2018**, *11*, 170. [Crossref]
70. Jaswal, T.; Gupta, J.; *Mater. Today: Proc.* **2021**, *81*, 859. [Crossref]
71. Ivlieva, A.; Petritskaya, E.; Rogatkin, D.; Yushin, N.; Grozdov, D.; Vergel, K.; Zinicovscaia, I.; *Appl. Sci.* **2022**, *12*, 3476. [Crossref]
72. Khan, M.; Khan, M. S. A.; Borah, K. K.; Goswami, Y.; Hakeem, K. R.; Chakrabartty, I.; *Environ. Adv.* **2021**, *6*, 100128. [Crossref]
73. Strużyńska, L.; Skalska, J. In *Cellular and Molecular Toxicology of Nanoparticles*; Saquib, Q.; Faisal, M.; Al-Khedhairy, A. A.; Alatar, A. A., eds.; Springer: Cham, 2018, p. 227. [Crossref]
74. Janzadeh, A.; Hamblin, M. R.; Janzadeh, N.; Arzani, H.; Tashakori-Miyanroudi, M.; Yousefifard, M.; Ramezani, F. In *Reviews of Environmental Contamination and Toxicology*, vol. 257; Springer: Cham, 2021, p. 93. [Crossref]
75. Li, L.; Bi, Z.; Hu, Y.; Sun, L.; Song, Y.; Chen, S.; Mo, F.; Yang, J.; Wei, Y.; Wei, X.; *Cell Biol. Toxicol.* **2021**, *37*, 177. [Crossref]
76. Suthar, J. K.; Vaidya, A.; Ravindran, S.; *J. Appl. Toxicol.* **2023**, *43*, 4. [Crossref]
77. Lujan, H.; Criscitiello, M. F.; Hering, A. S.; Sayes, C. M.; *Toxicol. Sci.* **2019**, *168*, 302. [Crossref]
78. Barosova, H.; Meldrum, K.; Karakocak, B. B.; Balog, S.; Doak, S. H.; Petri-Fink, A.; Clift, M. J. D.; Rothen-Rutishauser, B.; *Toxicol. In Vitro* **2021**, *75*, 105178. [Crossref]
79. ISO/TS Guide 19337: *Characteristics of Working Suspensions of Nano-Objects for in vitro Assays to Evaluate Inherent Nano-Object Toxicity*; ISO: Geneva, 2023.
80. Ribeiro, A. R.; Gemini-Piperni, S.; Travassos, R.; Lemgruber, L.; Silva, R. C.; Rossi, A. L.; Farina, M.; Anselme, K.; Shokuhfar, T.; Shahbazian-Yassar, R.; Borojevic, R.; Rocha, L. A.; Werckmann, J.; Granjeiro, J. M.; *Sci. Rep.* **2016**, *6*, 23615. [Crossref]
81. Partikel, K.; Korte, R.; Mulac, D.; Humpf, H.-U.; Langer, K.; *Beilstein J. Nanotechnol.* **2019**, *10*, 1002. [Crossref]
82. Pustulka, S. M.; Ling, K.; Pish, S. L.; Champion, J. A.; *ACS Appl. Mater. Interfaces* **2020**, *12*, 48284. [Crossref]
83. Yu, Q.; Zhao, L.; Guo, C.; Yan, B.; Su, G.; *Front. Bioeng. Biotechnol.* **2020**, *8*, 210. [Crossref]
84. Visalakshan, R.; González García, L. E.; Benzigar, M. R.; Ghazaryan, A.; Simon, J.; Mierczynska-Vasilev, A.; Michl, T. D.; Vinu, A.; Mailänder, V.; Morsbach, S.; Landfester, K.; Vasilev, K.; *Small* **2020**, *16*, 2000285. [Crossref]
85. Park, S. J.; *Int. J. Nanomed.* **2020**, *2020*, 5783. [Crossref]
86. Pu'ad, N. A. S. M.; Haq, R. H. A.; Noh, H. M.; Abdullah, H. Z.; Idris, M. I.; Lee, T. C.; *Mater. Today: Proc.* **2020**, *29*, 233. [Crossref]
87. Ghiasi, B.; Sefidbakht, Y.; Rezaei, M. In *Nanomaterials for Advanced Biological Applications*; Rahmandoust, M.; Ayatollahi, M. R., eds.; Springer Nature: Cham, 2019, p. 85. [Crossref]
88. Saxena, V.; Shukla, I.; Pandey, L. M.; *Materials for Biomedical Engineering*, 1st ed.; Holban, A.-M.; Grumezescu, A. M., eds.; Elsevier: London, UK, 2019, ch. 8. [Crossref]
89. Subramanian, R.; Sathish, S.; Murugan, P.; Musthafa, A. M.; Elango, M.; *J. King Saud Univ., Sci.* **2019**, *31*, 667. [Crossref]
90. Sotnikov, D. V.; Berlina, A. N.; Ivanov, V. S.; Zherdev, A. V.; Dzantiev, B. B.; *Colloids Surf., B* **2019**, *173*, 557. [Crossref]
91. Manzi, B. M.; Werner, M.; Ivanova, E. P.; Crawford, R. J.; Baulin, V. A.; *Sci. Rep.* **2019**, *9*, 4694. [Crossref]
92. Jain, A.; Trindade, G.; Hicks, J. M.; Pott, J. C.; Rahman, R.; Hague, R.; Amabilino, D. B.; Pérez-García, L.; Rawson, F.; *J. Colloid Interface Sci.* **2021**, *587*, 150. [Crossref]
93. Tang, M.; Gandhi, N. S.; Burrage, K.; Gu, Y.; *Langmuir* **2019**, *35*, 4435. [Crossref]
94. Smits, J.; Giri, R. P.; Shen, C.; Mendonça, D.; Murphy, B.; Huber, P.; Rezwan, K.; Maas, M.; *Langmuir* **2021**, *37*, 5659. [Crossref]
95. Mishra, R. K.; Ahmad, A.; Vyawahare, A.; Alam, P.; Khan, T. H.; Khan, R.; *Int. J. Biol. Macromol.* **2021**, *175*, 1. [Crossref]
96. Johnston, B. F.; Kreyling, W. G.; Pfeiffer, C.; Schäffler, M.; Sarioglu, H.; Ristig, S.; Hirn, S.; Haberl, N.; Thalhammer, S.; Hauck, S. M.; Semmler-Behnke, M.; Epple, M.; Hühn, J.; del Pino, P.; Parak, W. J.; *Adv. Funct. Mater.* **2017**, *27*, 1701956. [Crossref]
97. Ho, Y. T.; 'Ain Azman, N.; Loh, F. W. Y.; Ong, G. K. T.; Engudar, G.; Kriz, S. A.; Kah, J. C. Y.; *Bioconjug. Chem.* **2018**, *29*, 3923. [Crossref]
98. Li, X.; He, E.; Jiang, K.; Peijnenburg, W. J. G. M.; Qiu, H.; *Water Res.* **2021**, *190*, 116742. [Crossref]
99. Cotrut, C. M.; Vladescu, A.; Dinu, M.; Vranceanu, D. M.; *Ceram. Int.* **2018**, *44*, 669. [Crossref]
100. Li, N.; Xu, W.; Zhao, J.; Xiao, G.; Lu, Y.; *Thin Solid Films* **2018**, *646*, 163. [Crossref]

101. Zhu, Y.; Xu, L.; Liu, C.; Zhang, C.; Wu, N.; *AIP Adv.* **2018**, *8*, 085221. [Crossref]
102. López-Ortiz, S.; Mendoza-Anaya, D.; Sánchez-Campos, D.; Fernandez-García, M. E.; Salinas-Rodríguez, E.; Reyes-Valderrama, M. I.; Rodríguez-Lugo, V.; *J. Nanomater.* **2020**, *2020*, 5912592. [Crossref]
103. Meulendijks, N.; Van Ee, R.; Stevens, R.; Mourad, M.; Verheijen, M. A.; Kambly, N.; Armenta, R.; Buskens, P.; *Appl. Sci.* **2018**, *8*, 108. [Crossref]
104. Leong, S. S.; Ng, W. M.; Lim, J.; Yeap, S. P.; *Handbook of Materials Characterization*, 1st ed.; Sharma, S. K., ed.; Springer: Cham, Switzerland, 2018, ch. 8. [Crossref]
105. Hassan, P. A.; Rana, S.; Verma, G.; *Langmuir* **2015**, *31*, 3. [Crossref]
106. Brouzet, C.; Mittal, N.; Söderberg, L. D.; Lundell, F.; *ACS Macro Lett.* **2018**, *7*, 1022. [Crossref]
107. Quevedo, A. C.; Lynch, I.; Valsami-Jones, E.; *Nanoscale* **2021**, *13*, 6142. [Crossref]
108. De Matteis, V.; Cascione, M.; Toma, C. C.; Leporatti, S.; *J. Nanopart. Res.* **2018**, *20*, 273. [Crossref]
109. Martin, M. E.; Reaves, D. K.; Jeffcoat, B.; Enders, J. R.; Costantini, L. M.; Yeyeodu, S. T.; Botta, D.; Kavanagh, T. J.; Fleming, J. M.; *Nanomed.: Nanotechnol., Biol. Med.* **2019**, *21*, 102070. [Crossref]
110. Subbiah, R.; Jeon, S.; Park, K.; Yun, K.; Ahn, S.; *Int. J. Nanomed.* **2015**, *2015*, 191. [Crossref]
111. Montano, E.; Vivo, M.; Guarino, A. M.; di Martino, O.; Di Luccia, B.; Calabrò, V.; Caserta, S.; Pollice, A.; *Pharmaceuticals* **2019**, *12*, 72. [Crossref]
112. Saafane, A.; Durocher, I.; Vanharen, M.; Girard, D.; *Chem.-Biol. Interact.* **2022**, *365*, 110096. [Crossref]
113. Sthijns, M. M. J. P. E.; Thongkam, W.; Albrecht, C.; Hellack, B.; Bast, A.; Haenen, G. R. M. M.; Schins, R. P. F.; *Toxicol. In Vitro* **2017**, *40*, 223. [Crossref]
114. Chen, H.; Zhao, T.; Sun, D.; Wu, M.; Zhang, Z.; *Toxicol. In Vitro* **2019**, *56*, 84. [Crossref]
115. Pedrosa, M. S.; Alves, T.; Nogueira, F. N.; Holzhausen, M.; Sipert, C. R.; *Braz. Dent. J.* **2021**, *32*, 65. [Crossref]
116. Jin, X.; Zhuang, J.; Zhang, Z.; Guo, H.; Tan, J.; *J. Colloid Interface Sci.* **2015**, *443*, 125. [Crossref]
117. Yang, X.; Li, Y.; Liu, X.; Zhang, R.; Feng, Q.; *Stem Cells Int.* **2018**, *2018*, 2036176. [Crossref]
118. de Lima, I. R.; Alves, G. G.; Soriano, C. A.; Campaneli, A. P.; Gasparoto, T. H.; Ramos, E. S.; de Sena, L. Á.; Rossi, A. M.; Granjeiro, J. M.; *J. Biomed. Mater. Res., Part A* **2011**, *98A*, 351. [Crossref]
119. Bargon, S. D.; Gunning, P. W.; O'Neill, G. M.; *Biochim. Biophys. Acta, Mol. Cell Res.* **2005**, *1746*, 143. [Crossref]
120. Torrent, M.; Chalancon, G.; de Groot, N. S.; Wuster, A.; Babu, M. M.; *Sci. Signal.* **2018**, *11*, eaat6409. [Crossref]
121. ISO/TS Guide 21633: *Label-Free Impedance Technology to Assess the Toxicity of Nanomaterials in vitro*; ISO: Geneva, 2021.

Submitted: February 9, 2024
Published online: August 5, 2024